A Novel Experimental Model for Variable-Pitch Propellers

V.M. Arellano-Quintana[1,2], E.A. Merchan-Cruz[1], and Antonio Franchi[2]

***Abstract*—This paper proposes a new mathematical model to map the rotational speed and angle of attack (pitch) of small-size propellers typically used in multirotors and the aerodynamic thrust force and drag moment produced by the propeller itself. The new model is inspired by standard models using the blade-element and momentum theories, which have been suitably modified in order to allow for explicit fast computation of the direct and inverse map (useful for high-frequency control) and obtain a better adherence to experimental data. The new model allows and captures all the main nonlinear characteristics of the thrust/drag generation. An extensive experimental comparison shows that the prediction capability of the proposed model outperforms the most commonly used models at date. In the second part of the paper, two optimization methods are proposed in order to exploit the redundancy of the inputs of variable-pitch propellers to decrease the power consumption due to the drag dissipation. The first method deals with optimal allocation for thrust generation on a single propeller, while the second method is aimed at solving the optimal allocation of the rotational speed and pitch of all the propellers in a multi-rotor with any number of propellers. Simulations results show the viability and effectiveness of the proposed methods.**

I. Introduction

The fast growing of research in aerial robotics generates several new challenges that demand new approaches, such as, e.g., the one needed in physical interaction tasks with multi-rotors, see, e.g., [1]–[3]. In this paper we explore alternative models and solutions for the aerodynamic thrust generation problem faced in such emerging fields.

The use of variable pitch (VP) propellers is an alternative to the standard fixed-pitch (FP) propellers for several reasons. They are capable of changing the value of the thrust from positive to negative by using a combination of pitch angle and motor velocity. Therefore the set of admissible forces is enlarged, In fact, if we consider a standard quadrotor with FP propellers, the vehicle is not able to apply an arbitrary desired force downwards or even flip upside down; the maximum force that the vehicle can apply downwards corresponds to its own weight and perhaps less due to the minimum velocity required by the motors. However, thanks to the simplicity of building and controlling FP propellers, they are more popular for multirotors than the VP propellers.

[1]ESIME-UA, National Polytechnic Institute, Mexico City, Mexico, vicarellanoq@gmail.com,eamerchan@ipn.mx

[2]LAAS-CNRS, Université de Toulouse, CNRS, Toulouse, France, victor.arellano@laas.fr,antonio.franchi@laas.fr

This work has been partially funded by the European Unions Horizon 2020 research and innovation program under grant agreement No 644271 AEROARMS and Victor Arellano-Quintana has been funded by a scholarship from CONACyT for studies abroad.

The use of VP propellers in multirotors is not a new approach, they have been studied and implemented in the last years [4]–[8] as an alternative to the FP propellers. In [4], a comparison between FP propellers and VP propellers is done, they conclude that the VP propeller has a fundamental advantage of being able to change the direction of the thrust vector very fast. Also, they have found that VP propellers can track more accurately the velocity and acceleration commands. A complete study done by the same authors is presented in [6]. They analyze the effects of adding VP propellers in a quadrotor from the analytic part to the experimental part as well. They mention that the VP propellers are a quick method to reverse thrust. Similar conclusions and developments are presented in [5], [8].

Mathematical models that describe the aerodynamic effects of VP propellers have been developed in [8], [9]. Nevertheless, other approaches [10] have shown that the experimental results do not fit well with the mathematical models developed in these papers. In [10] an experimental model is proposed that claims to be more precise than the common models in the literature. However, the validation of the proposed model is only given for the thrust equation. Then, an approximation of the power consumed by the propeller is given and supported by experimental data.

On the other hand, one of the most known disadvantages of multirotors is the autonomy. VP propellers present one main advantage: they can save energy by allocating in a strategic way the pitch angle and the motor velocity. Therefore some approaches have been proposed to minimize the power consumption of the propeller using VP mechanism, see [10]–[12].

Despite the presence of these works, basic experimental research steps in the modeling of VP propellers are still strongly needed by the aerial vehicle community. In this paper, we aim at filling this gap by proposing a new mathematical model that is experimentally driven and validated. In Section II, we our proposed model and its theoretical basis. In Section III, the description of the experimental platform is given, and the parametric identification procedure is described. For sake of comparison, other models from the literature were identified as well. The comparison shows that the proposed model fits much better than the other models while having almost the same level of complexity. In Section IV, the drag optimization problem is stated. The optimization framework is tested in simulation on a fully-actuated hexa-rotor. Finally, the conclusions and the future work are presented in Section V.

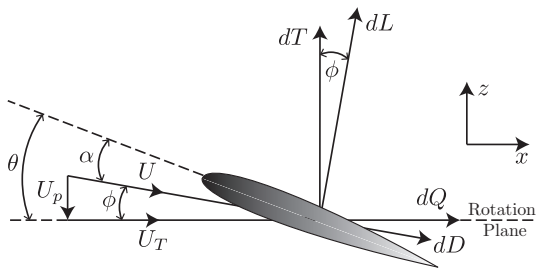

Fig. 1: Variable-Pitch scheme, where dL and dD are the resultant incremental lift and drag per unit span at the blade element, respectively; α is the angle of attack (AoA); ϕ is the relative inflow angle at the blade element.

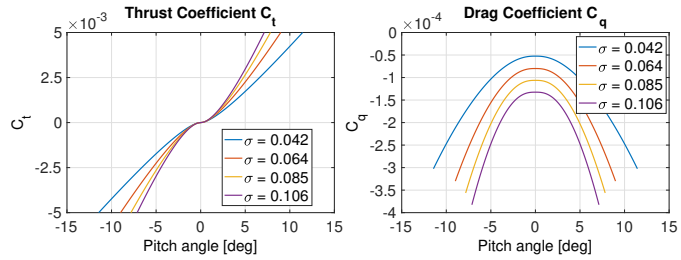

Fig. 2: a) Thrust coefficient C_t using the following values: $N = 2$, and $Cl_\alpha = 5.73$. b) Drag coefficient C_q curve using the same values for C_t and the zero-lift coefficient $C_{d_0} = 0.01$.

II. Variable-Pitch Propeller Aerodynamic Model

A. Theoretical Implicit Model for a Variable-Pitch Propeller

A VP propeller is a type of propeller which has a mechanism that allows varying the pitch angle θ of the rotor blades. This capability allows changing the thrust direction in both upward and downward directions by varying the pitch angle from positive to negative values. The thrust generated by a rotor is varied by changing either the blade pitch angle of the propeller or the spinning velocity. The relation between the lift (force) and the drag (moment) is derived using the blade element theory (BET) together with momentum theory, which is discussed in detail in [13], [14]. A scheme showing an element of the blade with its resultant forces is shown in Fig. 1. For helicopter rotors (see, e.g., [13]) one can assume that the out-of-plane velocity U_p is much smaller than the in-plane velocity U_T, and therefore $U \approx U_T$, leading to the fact that the angle ϕ is small. Therefore, a good approximation is that the increment in thrust (dT) and drag moment (dD) are approximately the increments in lift (dL) and torque (dQ) along the blade, respectively. By integrating the expressions for the thrust and the drag it is possible to derive the following model:

$$T = \rho C_t A(\omega R)^2 \tag{1}$$

$$Q = \rho C_q A(\omega R)^2 R \tag{2}$$

where T (in N) is the lift force (thrust); Q (in $\mathrm{N\,m}$) is the drag moment (or rotor-torque, simply called drag in the following); ω (in revolutions per second or better said in Hz) is the intensity of the angular velocity of the motor; R is the rotor radius; A is the area swept by the propeller; ρ is the air density (in $\mathrm{kg/m^3}$); C_t is the thrust coefficient; C_q is the drag coefficient. This model has been used in some papers like [7], [15], and it will be used as a guideline for the derivation of our the proposed model.

The thrust coefficient C_t is related to the shape of the propeller. Usually, the blades of FP propellers have a twist along the blade which lets the pitch angle change at each blade section. This is done to increase efficiency exploiting the fact that the induced velocity varies along the blade. However, in a VP propeller the blades are untwisted, i.e., θ is constant along the blade. Therefore, for blades with zero twist and considering uniform inflow velocity, the thrust coefficient is given implicitly by, see [13],

$$\theta = \frac{6C_t}{\sigma C_{l_\alpha}} + \frac{3}{2}\sqrt{\frac{|C_t|}{2}}\,\mathrm{sgn}(C_t) \tag{3}$$

where θ is the pitch angle (in rad); C_{l_α} is the 2D lift-curve-slope of the airfoil section(s) comprising the rotor; $\sigma = \frac{N_b c}{\pi R}$ is the blade solidity, where N_b is the number of blades, and c is the chord length. A plot using different values of blade solidity values is shown in Fig. 2a. Although the behavior of C_t is almost linear for high values of pitch angle, it can be seen the presence of a nonlinearity around zero, mainly due to the second term in (3), this term is the additional pitch required to compensate for the inflow resulting from the generated thrust.

Notice the absolute value in the squared root, this is necessary to account for negative values of thrust, the sign value of C_t is kept by the sign function. Furthermore, it can be seen that (3) is nonlinear, with no closed form inverse. Hence, in real-world applications, its inverse needs to be computed iteratively on-board, which may result unfeasible, since the control commands are sent at high frequency.

On the other hand, the drag coefficient is related to the thrust coefficient C_t, as follows,

$$C_q = \frac{|C_t|^{3/2}}{\sqrt{2}} + \frac{1}{8}\sigma C_{d_0} \tag{4}$$

where C_{d_0} is the zero-lift drag coefficient, this is caused by parasitic drag depending on the shape of the propeller. This term models the fact that even with zero pitch angle there is a drag moment, in contrast with what assumed in [6], where the drag value is considered proportional to the thrust. A plot of (4) using different values of blade solidity values is shown in Fig. 2b.

From (1)-(2) and (3)-(4) it can be seen that the computation of the thrust and drag, both essential for controlling a multi-rotor, is not straightforward, e.g., because (3) has be solved iteratively. Moreover, no force/torque sensors are considered in a UAV design due to the weight that would imply, and the high difficulty in properly filtering the noise induced by the vibrations. Therefore, a simpler model has to be used to precisely compute the thrust and drag generated by the propeller without the need of a sensorial feedback.

TABLE I: Principal VP models for multirotors reported in the literature.

Id	*Paper*	*Lift force Equation*	*Drag moment Equation*
i)	[5], [6]	$T = C^{i}_{T_1}\theta\omega^2$	$Q = -\operatorname{sgn}(\omega)(C^{i}_{Q_1}\omega^2 + C^{i}_{Q_2}\theta^2\omega^2 + C^{i}_{Q_3}\theta\omega)$
ii)	[8], [9]	$T = C^{ii}_{T_1}\theta\omega^2 - C^{ii}_{T_2}\omega$	$Q = C^{ii}_{Q_1}\omega^2 + C^{ii}_{Q_2}\omega^2\theta^2 + C^{ii}_{Q_3}\omega\theta + C^{ii}_{Q_4}$
iii)	[7], [13], [15]	$T = C^{iii}_{T_1}C_t\omega^2$ and $\theta = C^{iii}_{T_2}C_t + \frac{3}{2}\sqrt{\frac{\lvert C_t\rvert}{2}}\operatorname{sgn}(C_t)$	$Q = C^{iii}_{Q_1}\omega^2 C_t^{3/2} + C^{iii}_{Q_2}\omega^2$
iv)	[10]	$T = C^{iv}_{T_1}\lvert\sin_\theta\rvert\sin_\theta\,\omega^2$	No model presented.
v)	**proposed model**	$T = (\beta_1\lvert\sin_\theta\rvert\sin_\theta + \beta_2\sin_\theta)\omega^2 + (\beta_3\lvert\sin_\theta\rvert\sin_\theta + \beta_4\sin_\theta)\omega$	$Q = -\operatorname{sgn}(\omega)[(\gamma_1\sin^4_\theta + \gamma_2\sin^2_\theta + \gamma_3)\omega^2 + (\gamma_4\sin^4_\theta + \gamma_5\sin^2_\theta + \gamma_6)\omega$

B. Proposed Explicit Heuristic Model

In this section, the proposed experimental VP propeller model is introduced. We shall take as a guideline the theoretical model described in Section II-A. The motivation of arriving at a new model is mainly the simplicity for computing the thrust and drag generated by the VP propeller in real-world applications without the need of measuring the force/-torque online with additional onboard sensors. Therefore, the proposed model should be simpler and equally precise, and highly reliable for predicting thrust and drag values from the knowledge of the spinning velocity and the pitch angle.

1) Experimental Thrust Model: According to [16], the quadratic approximation of the thrust equation of a FP propeller commonly used in theory does not fit quite well with the experimental data. Therefore, they propose to approximate this thrust equation with a second-order polynomial in ω. However, in order to give physical sense to the equation, we can neglect the independent term. Hence, equation (1) can be rewritten as,

$$T = f_{C_t}(.)(\omega^2 + \omega) \tag{5}$$

where $f_{C_t}(.)$ is a function of the physical shape of the propeller and the pitch angle.

In the following we propose a new model of the thrust taking into account the pitch angle contribution. First of all, it can be seen that (3) is unbounded. However, this does not fit properly with reality, i.e., beyond a certain pitch angle value the lift begins to decrease, as it enters the stall condition. Hence, the equation to be found must possess the following characteristics:

- $f_{C_t}(.) \in \mathbb{R}$
- $f_{C_t}(\theta) = 0$, $\theta = 0$
- $f_{C_t}(\theta) = -f_{C_t}(-\theta)$ due to the reverse thrust.
- $f_{C_t}(.) \in [\underline{C}_t, \overline{C}_t]$

The function $f_{C_t}(.)$ proposed to model the thrust coefficient is the following:

$$f_{C_t}(\theta) = \beta_1\lvert\sin_\theta\rvert\sin_\theta + \beta_2\sin_\theta \tag{6}$$

where $\sin_\theta = \sin(\theta)$. Notice that the first term of (6) is a quadratic-like term which, however, has negative and positive values. Furthermore, the equation proposed has all the characteristics mentioned above.

Finally, the experimental thrust model that we propose has the following form:

$$\begin{aligned} T = \quad & (\beta_1\lvert\sin_\theta\rvert\sin_\theta + \beta_2\sin_\theta)\omega^2 + \\ & + (\beta_3\lvert\sin_\theta\rvert\sin_\theta + \beta_4\sin_\theta)\omega \end{aligned} \tag{7}$$

Equation (7) is slightly more complex than the one presented in [10]. However, the proposed equation will show to be much more precise and possessing a better prediction ability.

2) Experimental Drag Model: We take a similar approach to find an equation that relates the pitch angle and the drag moment. Taking (4), we replace the first term that it is related to the thrust coefficient C_t with a function dependent on the pitch angle. The function f_{C_q} to be found must possess the following characteristics:

- $f_{C_q}(.) \in \mathbb{R}$.
- $f_{C_q}(\theta) = C_{q,0}$, $\theta = 0$ due to the zero-lift coefficient.
- $f_{C_q}(\theta) = f_{C_q}(-\theta)$
- $f_{C_q}(.) \in [\underline{C}_q, \overline{C}_q]$

The function $f_{C_q}(.)$ proposed is the following:

$$f_{C_q}(\theta) = \gamma_1\sin^4_\theta + \gamma_2\sin^2_\theta + \gamma_3. \tag{8}$$

Notice that (8) is always convex (in the region of interest) and it is nonzero at any point, in order to model the zero-lift effect. Furthermore, the proposed model has all the characteristics mentioned above. Inspired by the relation between T and Q highlighted in (2) the proposed drag model takes the following form:

$$Q = -\operatorname{sgn}(\omega)f_{C_q}(.)(\omega^2 + \omega)$$

The term $-\operatorname{sgn}(\omega)$ accounts for the spinning direction of the propeller since it will generate torque in the opposite direction when the spinning direction changes its sign.

Rewriting the above equation and gathering all the constant terms in lumped coefficients, we obtain:

$$\begin{aligned} Q = \quad & -\operatorname{sgn}(\omega)[(\gamma_1\sin^4_\theta + \gamma_2\sin^2_\theta + \gamma_3)\omega^2 + \\ & + (\gamma_4\sin^4_\theta + \gamma_5\sin^2_\theta + \gamma_6)\omega]. \end{aligned} \tag{9}$$

III. Experimental Validation of the Proposed Model

A. Description of the Experimental setup

The experimental platform that we used for the testing and comparison is shown in Fig. 3 and its general characteristics are provided in Table II. It consists of a brushless (BL) motor[1], a VP mechanism[2] with a ten-inch propeller[3] attached and a micro servo with feedback[4]. The control is done in Matlab™

[1] http://wiki.mikrokopter.de/MK2832-35

[2] https://hobbyking.com/en_us/4d-hollow-variable-pitch-unit-without-motor-3mm-motor-shaft.html

[3] https://hobbyking.com/en_us/10-inch-replacement-blades-for-variable-pitch-motor-assembly.html

[4] https://www.adafruit.com/product/1404

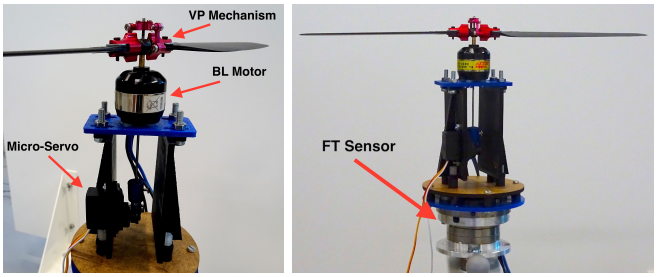

Fig. 3: Variable Pitch Testbed. The complete system is attached to a base by dampers in order to reduce vibrations. The main characteristics of the system are shown in Table II.

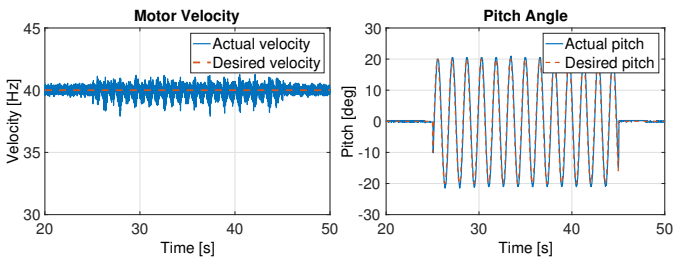

(a) (b)

Fig. 4: Velocity tracking while pitch angle tracks a sinusoidal.

by using a BL controller and an Arduino™ board for the micro servo. We used a Force/Torque (FT) sensor in order to measure the force and the moment generated by the VP propeller. The FT sensor is a SI-145-5, the full list of characteristics of the sensor can be found on its webpage[5]. The FT sensor was attached at the bottom of the platform as it is shown in Fig. 3-right. The angular velocity is measured using the zero crossings of the counter-electromotive force in the BL controller [17], which gives a precision of less than $\pm 0.1\,\mathrm{Hz}$. The pitch angle is measured by the servo encoder.

For controlling the pitch angle, a micro-servo with a linkage is used. A PI controller was implemented to precisely drive the blade pitch to its desired value. On the other hand, for controlling the rotational speed, a robust closed-loop controller presented in [17] was used. This controller provides a very good insensitivity to the perturbations caused by the pitch variations. In order to show its capability, we provide the results of the following stress test: a desired spinning velocity is kept constant at $40\,\mathrm{Hz}$ while the desired pitch angle is a sinusoidal trajectory going from its minimum to its maximum value ($-20\,\mathrm{deg}$ and $20\,\mathrm{deg}$) in less than $0.8\,\mathrm{s}$. This corresponds to an extremely large and fast variation of the disturbance torque for the motor controller. Despite such big disturbance, as we can see in Fig. 4, the motor controller [17] is capable of compensating these extreme perturbations and keep the tracking error within $\pm 1\,\mathrm{Hz}$.[6] Clearly, during the identification procedure, a much less aggressive trajectory was used, explained later, where the tracking error is a decimal fraction of the one seen in this stress test.

[5]http://www.ati-ia.com/products/ft/ft_models.aspx?id=Mini45

[6]The units in all the plots were changed from radians to degrees in order to facilitate the reading of the results.

TABLE II: Experimental platform specifications.

Component	*General Specifications*
VP Mechanism	Weight: $25\,\mathrm{g}$
Propeller size	Weight: $10\,\mathrm{g}$; Size: 10 inches
BL Motor	Weight: $68\,\mathrm{g}$; Max. Current: $10\,\mathrm{A}$
Microservo	Weight: $46\,\mathrm{g}$; Max. Torque: $2.1\,\mathrm{N\,m}$ at $6\,\mathrm{V}$
Force Sensor	Resolution: Force $1/16\,\mathrm{N}$; Torque $1/1504\,\mathrm{N\,m}$ Frequency: $1\,\mathrm{kHz}$

The relation between the blade pitch and the servo angle is non-linear, however, a proper function is defined to correlate both angles, this function works for calibrating the platform. The calibration was made using a special software for image analysis called Tracker[7]. Using this software different angular positions given to the micro-servo were recorded to find the counterpart for the blade pitch angle. After that, a proper function was approximated to find the relation between the two angles.

B. Parameter Identification Procedure

The identification is made offline using the least squares (LS) algorithm with outlier rejection in order to compute the coefficients for the different models in (7)-(9). The experiments were carried out in the following way: constant spinning velocities from $40\,\mathrm{Hz}$ to $80\,\mathrm{Hz}$ with steps of $10\,\mathrm{Hz}$ were set; in each step, while the spinning velocity was constant, the pitch angle tracked a ramp from $-20\,\mathrm{deg}$ to $20\,\mathrm{deg}$ in $20\,\mathrm{s}$. For the sake of comparison, four more VP models from the literature were also identified, a summary of these models is shown in the first four lines of Table I. Since the LS algorithm cannot be applied to model iii) because of its complexity, a stochastic optimization technique can be used to find the unknown coefficients; in particular, an evolutionary algorithm was used [18].

C. Identification Results and Model Comparison

After carrying out all the experiments, the parametric identification of the five models was performed. In the following, we present the numerical results. It is worth to mention that model i) is arguably the most used model in real applications. However, as it will be shown, its capability to predict the thrust and drag of the propeller is not fully satisfactory. The Root Mean Square Error (RMSE) was computed as a statistical indicator to have a fitness index for each model. They are gathered for the thrust and the drag of models i-v in Table III. The coefficients identified for the five models are listed in Table IV.

In order to provide a visual understanding the predictions and residual errors of the models i), ii), iii), and the proposed model v) are shown in two summarizing tables in Figs. 17 and 18, at the end of the paper. The predicted lift force of model iv) is very similar to the one of model iii) and therefore it is not reported here (quantitative results are reported in Table III).

[7]https://physlets.org/tracker/

TABLE III: Identification RMSE values for thrust and drag of all the models.

	Thrust [N]					Drag [N m]				
Velocity [Hz]	Model i)	Model ii)	Model iii)	Model iv)	Model v)	Model i)	Model ii)	Model iii)	Model iv)	Model v)
40	0.1986	0.1935	0.1505	0.1532	0.1115	0.0059	0.0044	0.0060	n/d	0.0034
50	0.2259	0.2092	0.1405	0.1449	0.1369	0.0041	0.0042	0.0046	n/d	0.0043
60	0.2949	0.2961	0.1641	0.1675	0.1693	0.0039	0.0043	0.0034	n/d	0.0041
70	0.4710	0.4665	0.2278	0.1620	0.1632	0.0062	0.0064	0.0058	n/d	0.0037
80	0.4486	0.4517	0.1868	0.2131	0.1613	0.0073	0.0067	0.0060	n/d	0.0024

TABLE IV: Identified coefficients of the five models.

Model id	*Thrust (lift force) coefficients*	*Drag (moment) coefficients*
i)	$C_{T_1} = 3.0503 \times 10^{-5}$	$C_{Q_1} = 6.2492 \times 10^{-7}$, $C_{Q_2} = 4.1604 \times 10^{-8}$, $C_{Q_3} = 1.2359 \times 10^{-6}$
ii)	$C_{T_1} = 3.0460 \times 10^{-5}$, $C_{T_2} = 7.4009 \times 10^{-4}$	$C_{Q_1} = 3.4568 \times 10^{-7}$, $C_{Q_2} = 4.1552 \times 10^{-8}$ $C_{Q_3} = 1.1954 \times 10^{-6}$, $C_{Q_4} = 4.4 \times 10^{-3}$
iii)	$C_{T_1} = 0.0190$, $C_{T_2} = 3.9865$	$C_{Q_1} = 2.4 \times 10^{-3}$, $C_{Q_2} = 9.0679 \times 10^{-7}$
iv)	$C_{T_1} = 6.6 \times 10^{-3}$	n/c
v)	$\beta_1 = 4.7804 \times 10^{-3}$, $\beta_2 = 2.8394 \times 10^{-4}$, $\beta_3 = 4.5704 \times 10^{-2}$, $\beta_4 = 2.2233 \times 10^{-3}$	$\gamma_1 = 1.0131 \times 10^{-3}$, $\gamma_2 = 3.5109 \times 10^{-6}$, $\gamma_3 = 1.1091 \times 10^{-6}$, $\gamma_4 = -1.1542 \times 10^{-2}$, $\gamma_5 = 3.2645 \times 10^{-3}$, $\gamma_6 = 4.1655 \times 10^{-5}$

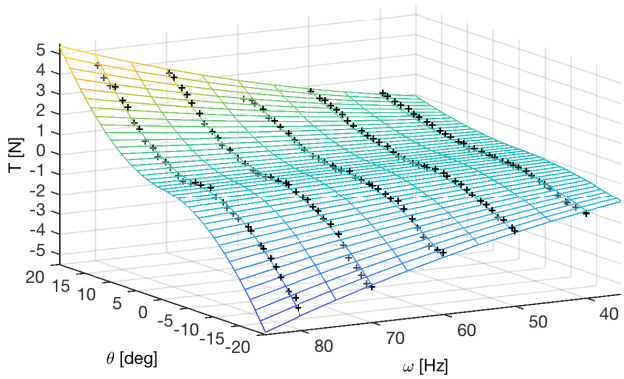

Fig. 5: Thrust evaluation using the proposed model v).

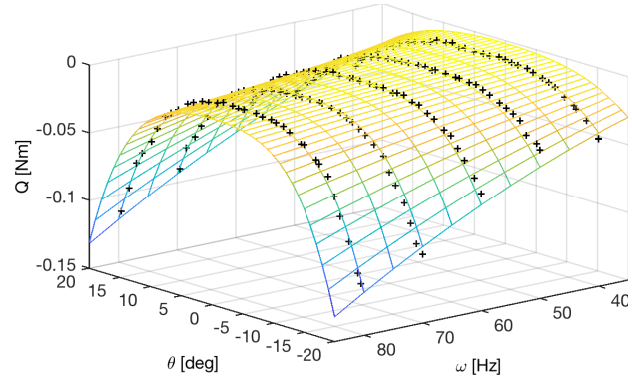

Fig. 6: Drag evaluation using the proposed model v).

Model i) is arguably the most popular model for multirotors at the date. However, from the RMSE and the plots it is clear that the experimental results agree with model i) neither quantitatively nor qualitatively. In fact, at constant spinning velocity model i) predicts a linear behavior on the thrust with respect to the pitch angle, however, a nonlinear behavior is clearly seen experimentally. Although the linear approximation of the pitch angle could be useful for applications in which larger angles of the pitch are required and just a quick switch through zero is needed, for other applications, it is mandatory to have a precise prediction of the thrust and drag around the zero pitch. Also, the shape of the predicted drag fits unsatisfactorily with the experimental data. The proposed model v) fits much better both for thrust and drag. In fact, thanks to its nonlinearity, the region around zero is predicted very nicely.

The good quality of the model proposed can be also compared with the other three common models ii), iii), and iv), by observing the RMSE values reported in Table III. It is possible to see how the RMSE values of the proposed model are significantly smaller than the others, despite its equivalent complexity[8].

Finally, Figs. 5 and 6 provide a global overview of the powerfulness of the proposed model by showing the experimental data superimposed to the full 3D surfaces for models (7) and (9), respectively, as functions of ω and θ.

IV. Drag Optimization

A. Power dissipation

Brushless Direct Current (BLDC) motors are the most common type of motors used in multirotors. BLDC motors have high efficiency, high torque-to-weight ratio, increased reliability, reduced noise and longer lifetime. Although the mathematical model of a BLDC motor has three equations due to its three-phase permanent magnet motor, it can be approximated by a permanent magnet direct current motor. A simplified model of a DC motor is the following

$$E_m(t) = R_a i_a(t) + K_e \omega(t) \quad (10)$$

$$i_a(t) = \frac{1}{K_T}\left[(J_m + J_L)\dot{\omega}(t) + T_m + T_L\right] \quad (11)$$

[8]Notice that model iii) is even more complex than the proposed one, since it needs to solve three equations in order to compute the thrust and drag.

where $E_m(t)$ [V] is the supply voltage; $i_a(t)$ [A] is the current trough the motor coils; R_a [Ω] is the armature resistance; K_e is the motor back EMF constant [V s/rad]; K_T [N m/A] is the motor torque constant; $\omega(t)$ [rad/s] is the angular velocity of the motor that coincides with the velocity of the load; J_m and J_L are the moment of inertia of the motor and the load, respectively; T_m is the opposing torque due to the Coulomb and viscous friction, and T_L is the torque due to the load. According to [19], the motor torque constant K_T [N m/A] is theoretically equal to K_e.

The input power to the motor $P_i(t)$ is given by,

$$\begin{aligned} P_i(t) &= i_a^2(t)R_a + K_e\omega i_a(t) \\ &= i_a^2(t)R_a + \omega(t)T_m + \omega(t)T_L + \\ &\quad +(J_m + J_L)\omega(t)\dot{\omega}(t). \end{aligned} \tag{12}$$

Therefore, we can identify three terms that can be considered as power losses in a DC motor on the right-hand-side of (12). These can be due to electrical or mechanical reasons,

- $i_a^2(t)R_a$ - Winding resistive loss.
- $\omega(t)T_m$ - Coulomb friction and viscous friction.
- $\omega(t)T_L$ - Load dissipation.

Notice that the last term in (12) can be ignored when either the velocity is constant (or slowly varying) or where the final velocity and the initial velocity are equal over an interval.

By definition, the propeller drag is considered as the load of the motor T_L, therefore, if the load is minimized, the part of the power due to load dissipation, which constitutes a large portion of the total power, will be minimized as well.

Supported by the previous analysis, in the following, we tackle the problem of minimizing the VP-propeller drag Q while producing the desired thrust for a single rotor (Sec. IV-B) or a desired total wrench (Sec. IV-C) for a fully-actuated multi-rotor system.

B. Optimal Drag Problem for a Single Rotor

Figure 7 shows the isothrust and isodrag curves in the plane ω-θ for the identified setup of Figure 3. Such curves are defined as the level curves of the functions T and Q in (7) and (9) respectively. It can be seen that many isodrag curves intersect an isothrust curve, i.e., several values of drag can be generated for one value of thrust. Motivated by the power consumption discussion in the previous section we consider then the problem of choosing the spinning velocity ω and the pitch angle θ in order to obtain a desired thrust T_* while minimizing the absolute value of the drag $|Q|$, according to the proposed and validated model.

The VP-propeller drag is characterized by (9), that we validated and compared experimentally. The identified coefficients for our experimental platform are shown in Table IV. In Fig. 8 we show the corresponding drag curves for constant values of thrust ranging from 0.5 N to 5 N. The curves are obtained from (9) by varying $\theta \in (0, 20]$ continuously and computing ω from (7) for the particular θ and the given constant value of T. It can be seen that such curves are convex with respect to θ in that range. Moreover, the unconstrained minimum value is always close 10 deg, for the particular setup in Figure 3.

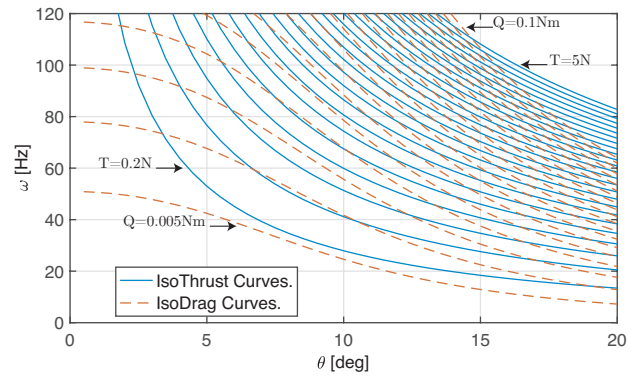

Fig. 7: Isothrust and isodrag curves. Isothrust curves have a step of 0.2 N from 0.2 N to 5 N. Isodrag curves have a step of 0.005 N m from 0.005 N m to 0.1 N m.

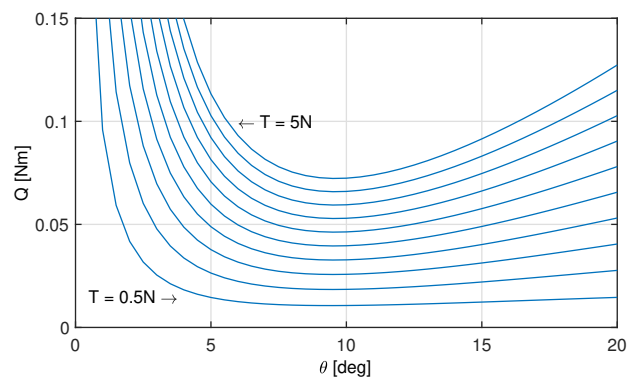

Fig. 8: Isothrust drag curves. The thrust step is 0.5 N.

Other setup might present different behaviors, while convexity is always preserved.

In this case, one single motor-propeller is considered. We are interested in finding the combination of pitch angle θ and the motor velocity ω that generate a desired value of thrust T_* such that (9) is minimum. The problem is multi-variable, however, it can be rewritten as a single variable optimization problem by doing some algebra.

Let be given a desired thrust $T_* > 0$ (if $T_* < 0$ then the problem can be solved for $-T_*$ and then the sign of the found θ_* can be flipped; if $T_* = 0$ the solution is $\omega = 0$ with any θ). The goal is to find θ^* and ω^* that realize $T = T_*$ and minimize $|Q|$.

First of all since $Q(\omega, \theta) = Q(-\omega, \theta)$ any minimum that can be reached with a $\omega < 0$ can also be reached with the opposite positive ω. Second of all since $T(\omega, \theta) = T(-\omega, -\theta)$ any thrust that can be realized with $\omega < 0$ can also be realized with the opposite (positive) ω and the opposite θ. Therefore, considering also that $T_* > 0$ and observing the shape of T w.r.t. θ we can restrict the optimization problem to case in which $\omega > 0$ and $0 < \theta < \pi/2$. Given this assumption we

have that,

$$
\begin{aligned}
T &= (\beta_1|\sin_\theta|\sin_\theta + \beta_2 \sin_\theta)\omega^2 + \\
&\quad +(\beta_3|\sin_\theta|\sin_\theta + \beta_4 \sin_\theta)\omega \\
&= g_{T_1}(\theta)\omega^2 + g_{T_2}(\theta)\omega, \qquad (13)\\
Q &= -(\gamma_1 \sin_\theta^4 + \gamma_2 \sin_\theta^2 + \gamma_3)\omega^2 - \\
&\quad -(\gamma_4 \sin_\theta^4 + \gamma_5 \sin_\theta^2 + \gamma_6)\omega \\
&= g_{Q_1}(\theta)\omega^2 + g_{Q_2}\omega, \qquad (14)
\end{aligned}
$$

where $g_{T_1}(\theta), g_{T_2}(\theta)$ and $g_{Q_1}(\theta), g_{Q_2}(\theta)$ are positive and monotone functions in the domain of interest. The problem to solve is then,

$$
\begin{aligned}
\min_{\theta,\omega} \quad & Q(\omega,\theta) \\
\text{s.t.} \quad & \underline{\theta} \le \theta \le \overline{\theta}, \\
& \underline{\omega} \le \omega \le \overline{\omega}, \\
& T(\omega,\theta) = T_*
\end{aligned} \qquad (15)
$$

where $0 < \underline{\theta} < \overline{\theta} < \pi/2$ and $0 < \underline{\omega} < \overline{\omega}$.

Solving for $\omega_*(\theta)$ with $T = T_*$ in (13) and substituting in Q we can eliminate the variable ω and the equality constraint. Furthermore we can replace the inequality constraint on ω in an inequality constraint on θ by imposing that $\underline{\omega} \le \omega_*(\theta) \le \overline{\omega}$. We solve for θ_a in (13) with T_* and $\overline{\omega}$, and θ_b with T_* and $\underline{\omega}$. Denoting with $\theta_1 = \max(\theta_a, \underline{\theta})$ and $\theta_2 = \min(\theta_b, \overline{\theta})$ we can reformulate the minimization as

$$
\begin{aligned}
\min_{\theta} \quad & Q(\omega,\theta) \\
\text{s.t.} \quad & \theta_1 \le \theta \le \theta_2
\end{aligned} \qquad (16)
$$

notice that T_* does not play any role in the cost function but only in the definition of the constraints on θ.

Now, problem (16) can be solved with a single-variable unconstrained optimization method, for instance, the dichotomy algorithm. This algorithm is simple but efficient for solving a problem in which the function is convex and unimodal. Moreover, it does not require either gradient or Hessian information, and allow computing the required iterations given the step and tolerance. This last is useful for real-applications since the exact number of iterations need to ensure the convergence of the algorithm is set. In Algorithm 1, the pseudo-code is shown.

Algorithm 1: Single rotor optimization

1. Compute $\omega_*(\theta)$ with T_* using (13);
2. Substitute $\omega_*(\theta)$ in (14);
3. Solve θ_a and θ_b with T_* using (13) and the constraints in ω;
4. Define the constraints θ_1 and θ_2;
5. Solve the optimization problem (16);

Results: In order to show that the algorithm is able to find the minimum value of Q for, e.g., the identified setup of Figure 3, the algorithm has been tested for fixed values of thrust $Td = [0.2, 0.4, 0.6, 0.8, 1]$, and then the isothrust curves will be plotted together with the isocurves found by the algorithm, see Fig. 9.

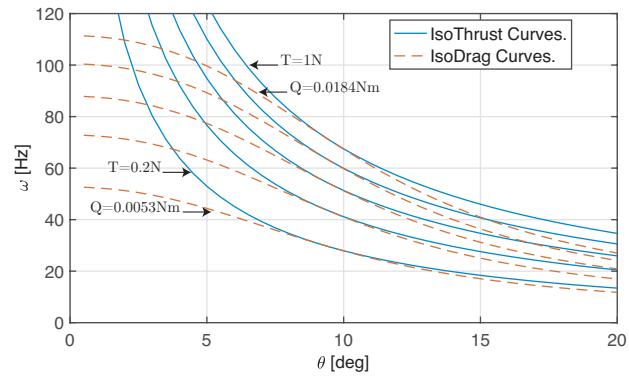

Fig. 9: Isothrust curves and the isodrag curves found by the algorithm with the following values of desired thrust $Td = [0.2, 0.4, 0.6, 0.8, 1]$.

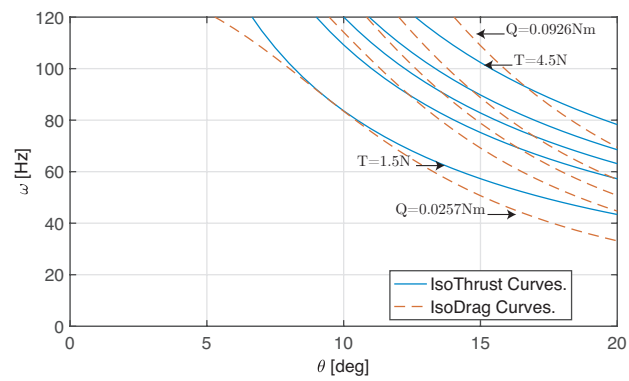

Fig. 10: Isothrust curves and the isodrag curves found by the algorithm with the following values of desired thrust $T_d = [1.5, 2, 3, 4, 4.5]$.

The vector of optimal pitch angles, the vector of motor velocities and the vector of the function Q were the following,

$$
\begin{aligned}
T_d &= [0.2, 0.4, 0.6, 0.8, 1] \\
\theta^* &= [9.3630, 9.3767, 9.4107, 9.4392, 9.4623] \\
\omega &= [29.7823, 43.7286, 54.3084, 63.1875, 70.9899] \\
|Q|^* &= [0.0053, 0.0089, 0.0122, 0.0154, 0.0184]
\end{aligned}
$$

Furthermore, the optimal values of pitch angles and motor velocities for higher values of thrust are presented,

$$
\begin{aligned}
T_d &= [1.5, 2, 3, 4, 4.5] \\
\theta^* &= [9.5604, 11.0602, 13.5764, 15.6976, 16.6580] \\
\omega &= [87.0964, 88.7046, 90.8413, 92.2991, 92.8909] \\
|Q|^* &= [0.0257, 0.0507, 0.0531, 0.0781, 0.0926].
\end{aligned}
$$

As it can be seen from Fig. 10, the drag values found by the algorithm for higher values of thrust would be suboptimal for the unconstrained problem, in fact, the isothrust and isodrag curves found by the algorithm are not tangent. However the values found are optimal for the constrained problem. If the upper bound of the motor velocity was higher, for instance, $20 < \omega < 150$, the optimal values of pitch angles would be located around $11\,\text{deg}$.

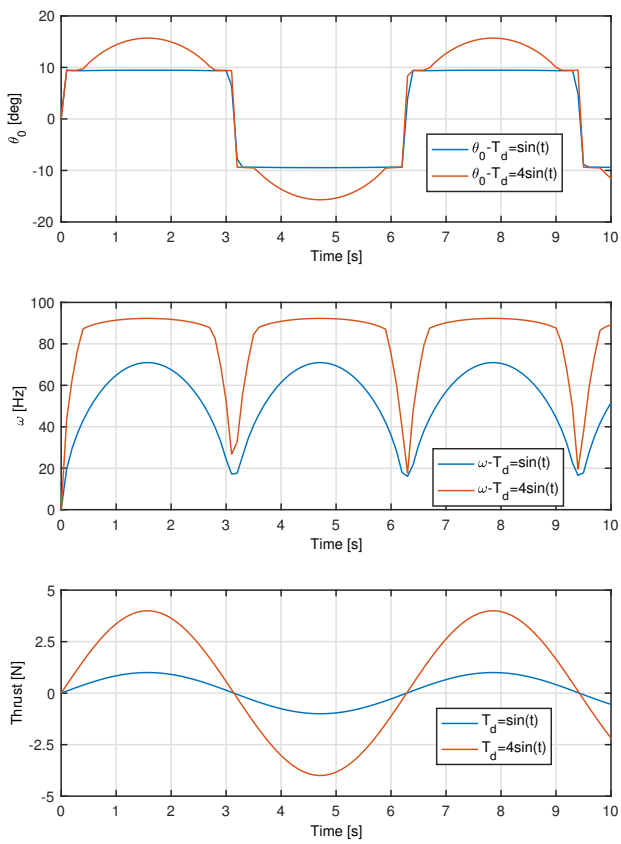

Fig. 11: Single VP propeller optimization.

Now, two sinusoidal signals are taken as desired thrust $T_{d_1} = \sin_t$ and $T_{d_2} = 4\sin_t$, to analyze the behavior of the commanded pitch angle and motor velocity.

In the first case, the pitch angle remains almost the same around $10\,\text{deg}$ since the required motor velocity is within its valid range. On the other hand, in the second case the pitch angle changes at the moment in which the motor velocity reaches its upper bound, leading to an increment in the pitch angle to achieve the desired thrust, while still minimizing the drag, see Fig. 11. In other words, the pitch angle remains almost constant if the motor velocity values are within its limits, otherwise, the motor velocity goes up to upper limit and the pitch angle finishes the job.

C. Optimal drag for a fully-actuated multi-rotor

The dynamics of an n-rotor can be described by the following matrix equation,

$$\underbrace{\begin{bmatrix} m\mathbf{I}_3 & \mathbf{0}_3 \\ \mathbf{0}_3 & \mathbf{J} \end{bmatrix}}_{\mathbf{M}} \underbrace{\begin{bmatrix} \ddot{\mathbf{p}} \\ \dot{\boldsymbol{\omega}} \end{bmatrix}}_{\mathbf{a}} = \underbrace{\begin{bmatrix} -mg\hat{\mathbf{z}} \\ -\boldsymbol{\omega} \times \mathbf{J}\boldsymbol{\omega} \end{bmatrix}}_{\mathbf{f}} + \underbrace{\begin{bmatrix} \mathbf{R}_r & \mathbf{0}_3 \\ \mathbf{0}_3 & \mathbf{I}_3 \end{bmatrix}}_{\mathbf{B}} \underbrace{\begin{bmatrix} \mathbf{F}_1 \\ \mathbf{F}_2 \end{bmatrix}}_{\mathbf{F}} \mathbf{u} \quad (17)$$

where n is the number of rotors. Matrix $\mathbf{F}$ is the allocation matrix of the total wrench applied to the multirotor; matrices $\mathbf{F}_1$ and $\mathbf{F}_2$ are the force and moment matrices, respectively. Matrix $\mathbf{F}_1 \in \mathbb{R}^{3\times n}$ is made by unit vectors $\mathbf{v}_i \in \mathbb{R}^{3\times 1}$ that define the orientation of the propeller i, $||\mathbf{v}_i|| = 1$. Matrix $\mathbf{F}_2 \in \mathbb{R}^{3\times n}$ is made by the vectors $\mathbf{w}_i \in \mathbb{R}^{3\times 1}$ that define the sum of the torque due to thrust and the torque due to drag moment, i.e. $\mathbf{w}_i = \sigma_i k_{d_i}\mathbf{v}_i + \mathbf{r}_i \times \mathbf{v}_i$, where $\mathbf{r}_i$ is the position vector of propeller i to the center of gravity of the vehicle; k_m is a coefficient that relates the spinning velocity with the torque produced around the rotation axis, and σ_i is the direction of rotation $\sigma_i \in \{-1, 1\}$. To compensate the torque (drag moment) of each propeller the value of σ_i is defined as $\sigma_i = -1^i$. The control input is the force generated by the propeller $\mathbf{u} = [f_1, .., f_6]^T$. Following the parametrization presented in [20], the propeller angles used in this work are $\alpha = \pm 35\,\text{deg}$ and $\beta = 10\,\text{deg}$.

The control allocation matrix $\mathbf{F}$ maps from the propellers thrust to the forces and torques applied to the hexa-rotor. Therefore, the matrix $\mathbf{F}$ can be expressed as follows,

$$\mathbf{F} = \begin{bmatrix} \mathbf{F}_1 \\ \mathbf{F}_2 \end{bmatrix} = \begin{bmatrix} \mathbf{F}_1 \\ \mathbf{P} \times \mathbf{F}_1 + \mathbf{Q} \end{bmatrix} \quad (18)$$

where $\mathbf{F}_1$ is a matrix made by the propellers orientation; $\mathbf{F}_2$ is the moment allocation matrix; $\mathbf{P}$ is the matrix that contains the position of the propellers and $\mathbf{Q}$ is the drag due the VP propellers, defined as,

$$\mathbf{Q} = \left[k_{d_1}\mathbf{v}_1, ..., k_{d_6}\mathbf{v}_6\right] \quad (19)$$

where k_{d_i} is the relation between the drag generated by the VP-propeller and the force, $k_{d_i} = Q_i^*/(f_i + \gamma)$ where γ is for avoiding indetermination, sufficiently small to not affect the value of Q_i^*. The controller used in this simulations is a Feedback Linearization with a PID controller. The PID controller is defined as follows,

$$\mathbf{w}_d = -\mathbf{f} - \mathbf{K}_p\mathbf{e}_p - \mathbf{K}_d\dot{\mathbf{e}}_p - \mathbf{K}_i\int_{t_0}^{t_f}\mathbf{e}_p dt + \mathbf{a}_d \quad (20)$$

where matrices $\mathbf{K}_p, \mathbf{K}_d, \mathbf{K}_i \in \mathbb{R}^{6\times 6}$ are diagonal matrices with proper proportional, derivative and integral gains, respectively; the errors in translation and orientation are defined as follows,

$$\mathbf{e}_p = \begin{bmatrix} \mathbf{e}_{pos} \\ \mathbf{e}_{att} \end{bmatrix} = \begin{bmatrix} \mathbf{p} - \mathbf{p}_r \\ \frac{1}{2}(\mathbf{R}_d^T\mathbf{R}_r - \mathbf{R}_r^T\mathbf{R}_d) \end{bmatrix} \quad (21)$$

$$\dot{\mathbf{e}}_p = \begin{bmatrix} \dot{\mathbf{e}}_{pos} \\ \mathbf{e}_\omega \end{bmatrix} = \begin{bmatrix} \dot{\mathbf{p}} - \dot{\mathbf{p}}_r \\ \boldsymbol{\omega} - \mathbf{R}_r^T\mathbf{R}_d\hat{\boldsymbol{\omega}}_r \end{bmatrix} \quad (22)$$

where $\hat{(.)}$ is the hat operator; $\boldsymbol{\omega}_r = \mathbf{R}_d^T\dot{\mathbf{R}}_d$.

The control allocation strategy is simple since the matrix $\mathbf{F}$ is full rank, the control allocation is made by just inverting it as follows,

$$\mathbf{u} = (\mathbf{M}^{-1}\mathbf{B}\mathbf{F})^{-1}\mathbf{w}^*. \quad (23)$$

Using this controller, the matrix $\mathbf{F}$ is required to have inverse in order to know the force required by each propeller. The approach we propose to solve the problem of the fully-actuated hexa-rotor with VP-propellers in an optimal sense is to find the matrix $\mathbf{F}$ iteratively by using single rotor optimization problem presented in Section IV-B for each motor, this algorithm was inspired by the one proposed in [16]. First-of-all, the algorithm initiate by computing the total thrust desired f, in this case, we assume that the total thrust is defined as $f = mg$, where m is

the hexa-rotor mass. Then, we compute the initial force needed by each VP-propeller as $f_{1,\ldots,6} = (\mathbf{M}^{-1}\mathbf{BF})^{-1}\mathbf{w}^*$ with $\mathbf{w}^* = [0, 0, mg, 0, 0, 0]^T$. After that, six optimization problems are solved having as desired thrust the forces found in the previous step. By solving the six optimization problems we get the (minimum) drag produced by each propeller, $Q_1^*, \ldots, Q_6^*$, these values are substituted in matrix $\mathbf{F}$ and then its inverse is computed, finally the forces values now become the initial forces, and the algorithm starts again, see Algorithm 2 for the pseudocode.

Algorithm 2: Matrix $\mathbf{F}$ computation

Compute initial forces $f_{1,\ldots,6} = (\mathbf{M}^{-1}\mathbf{BF})^{-1}\mathbf{w}^*$ with $\mathbf{w}^* = [0, 0, mg, 0, 0, 0]^T$;
for $k = 1$ *to* k_{end} **do**
  Solve optimization problem from Section IV-B for each f_i and save the optimal values of Q_i^*;
  Compute matrix $\mathbf{F}$ using Q_i^* values ;
  Compute $\mathbf{F}^{-1}$ and find the required forces for the desired total thrust f_d and the desired torques $\mathbf{M}_d$;
end

After a few steps, the propeller forces converge to the proper values to produce the required total thrust and the required torques, minimizing the drag. The algorithm is suitable to be implemented online, since the time required to compute Algorithm 2 is lower than the typical control period of $2\,\mathrm{ms}$.

D. Results

In this section we present a comparison with the main strategy used in the literature in which the velocity is kept constantly at its maximum value [5], [6], [8], [11]. Such strategy generates the desired thrust by varying the pitch angle, and the relation between force and pitch becomes one to one. The same simulation with the same trajectory, parameters and control gains with such strategy is run and compared with our method. In order to have more realistic simulation results, we added Gaussian white noise to the measurements. In addition, to show the effectiveness of the method, we defined the following performance index,

$$J_q = \int_{t_0}^{t_f} \sum_{i=1}^{6} |Q_i| dt. \tag{24}$$

This is equivalent to sum the absolute values of the drag of the six VP-propellers over time.

In Figs. 12-14, it can be seen, that the tracking is similar in the two cases, and the forces demanded by the controller are similar as well. In Figs. 13-15, it can be seen that the optimization strategies minimize the drag consumption, going to almost zero values in some points. On the other hand, in the non-optimized case (constant speed) it is not possible to reduce the drag below a certain value, even if a zero force is required.

However, the performance indexes are different between the two methods, see Fig. 16. Taking the final values, i.e. the total drag over time, the difference is around $2.9834\,\mathrm{N\,m\,s}$.

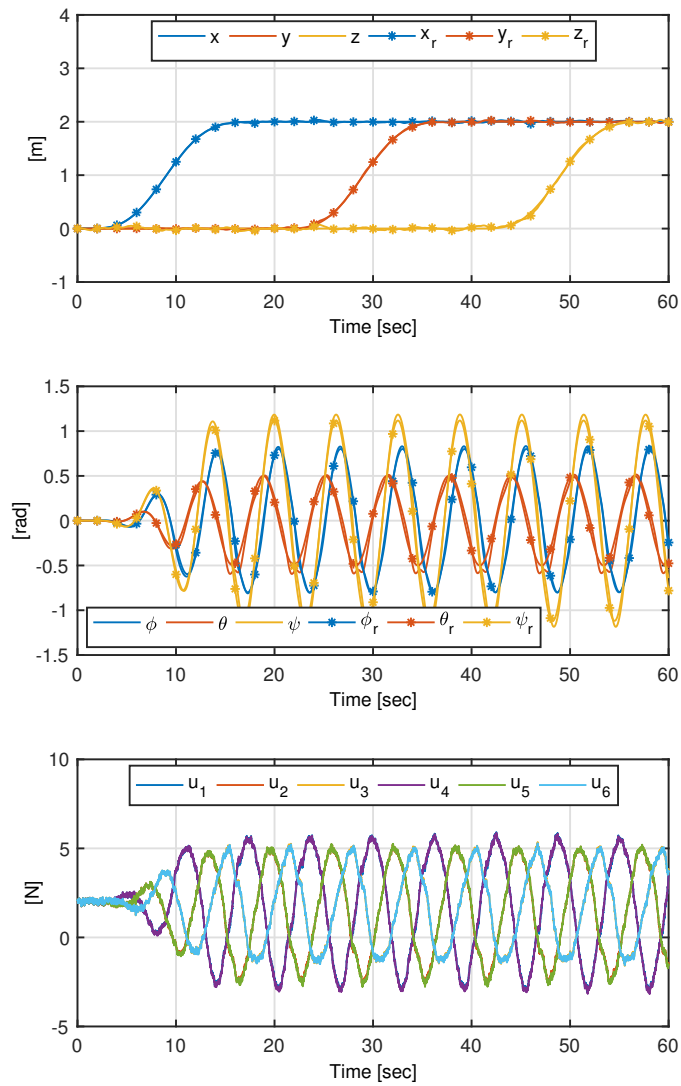

Fig. 12: Trajectory tracking by a hexa-rotor with VP-propellers using the proposed optimization strategy.

V. Conclusions and Future Work

Making use of the commonly accepted blade element theory, we proposed a mathematical model for variable-pitch propellers employed in multirotors. The main goal was to get a simpler model, that is fast enough to be solved in real-time applications and precise enough to predict the thrust/drag values without the necessity of force/torque sensors onboard. The proposed model was experimentally compared with the four most popular models in the literature. Despite the fact that the proposed model is equivalent to the most popular ones in terms of complexity, the comparison has shown that it is significantly more precise in terms of fitting and force/torque prediction. The RMSE values obtained with the proposed model are less than $0.18\,\mathrm{N}$ in all the cases for the thrust and less than $0.0045\,\mathrm{N\,m}$ for the drag, for the identified setup of Figure 3. Furthermore, we proposed an algorithm that optimizes the power loss due to the drag of the propellers, the algorithm was successfully tested in simulation on single

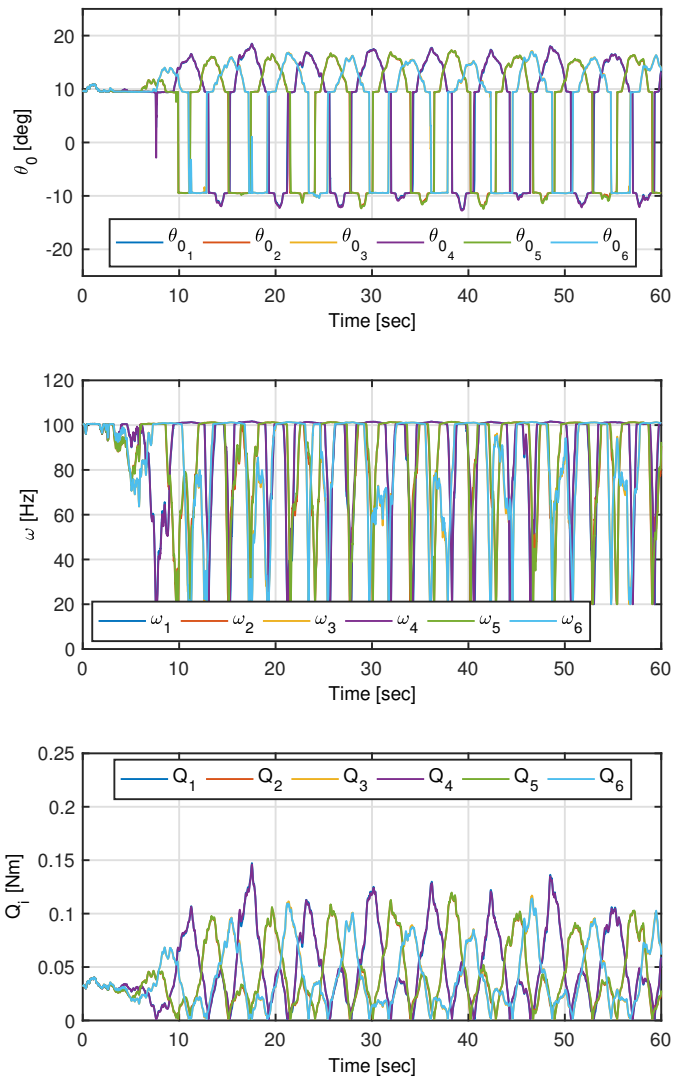

Fig. 13: Optimal values of the pitch, the motor velocities and the drag for each rotor using the proposed optimization strategy.

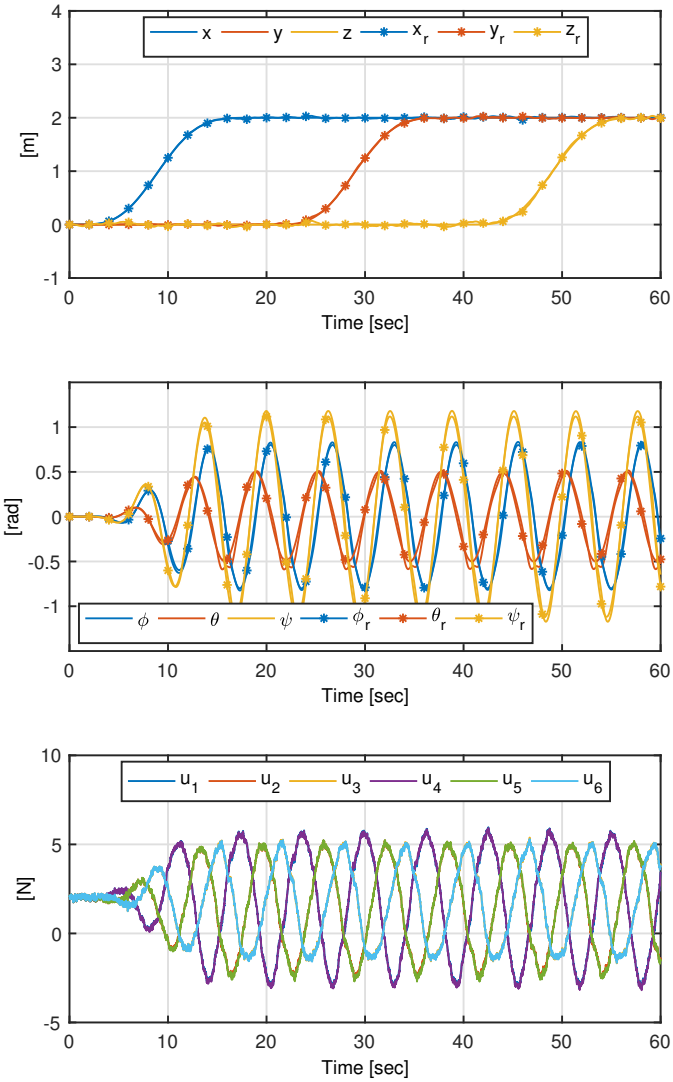

Fig. 14: Trajectory tracking by a hexa-rotor with VP-propellers, without using the optimization strategy (constant speed).

propeller and on a fully-actuated hexa-rotor; this kind of platforms are more suitable for having optimization strategies with VP propellers, since even in hover condition the required thrust variation is larger than in a quadrotor. Based on this fundamental building block, in the future, we will work on control laws for energy efficient consumption strategies and use this proposed model to drive multirotors in physically interactive tasks.

Acknowledgment

Victor Arellano-Quintana would like to thank CONACYT for the scholarship granted in pursuit of his doctoral studies and COFAA for the funding.

References

[1] M. Ryll, G. Muscio, F. Pierri, E. Cataldi, G. Antonelli, F. Caccavale, and A. Franchi, "6d physical interaction with a fully actuated aerial robot," in *IEEE International Conference on Robotics and Automation (ICRA)*, 2017.

[2] N. Staub, D. Bicego, Q. Sablé, V. Arellano, S. Mishra, and A. Franchi, "Towards a flying assistant paradigm: the othex," in *IEEE International Conference on Robotics and Automation (ICRA)*, 2018.

[3] K. Kondak, A. Ollero, I. Maza, K. Krieger, A. Albu-Schaeffer, M. Schwarzbach, and M. Laiacker, "Unmanned aerial systems physically interacting with the environment: Load transportation, deployment, and aerial manipulation," in *Handbook of Unmanned Aerial Vehicles*. Springer, 2015, pp. 2755–2785.

[4] M. Cutler, N. K. Ure, B. Michini, and J. P. How, "Comparison of fixed and variable pitch actuators for agile quadrotors," *AIAA Paper*, vol. 2, no. 2011-6406, 2011.

[5] A. Pretorius and E. Boje, "Design and modelling of a quadrotor helicopter with variable pitch rotors for aggressive manoeuvres," *IFAC Proceedings Volumes*, vol. 47, no. 3, pp. 12 208–12 213, 2014.

[6] M. Cutler and J. P. How, "Analysis and control of a variable-pitch quadrotor for agile flight," *Journal of Dynamic Systems, Measurement, and Control*, vol. 137, no. 10, pp. 101 002–1 –101 002–14, 2015.

[7] N. Gupta, M. Kothari *et al.*, "Flight dynamics and nonlinear control design for variable-pitch quadrotors," in *2016 American Control Conference (ACC)*. IEEE, 2016, pp. 3150–3155.

[8] R. Porter, B. Shirinzadeh, and M. H. Choi, "Experimental analysis of variable collective-pitch rotor systems for multirotor helicopter applications," *Journal of Intelligent & Robotic Systems*, vol. 83, no. 2, pp. 271–288, 2016.

[9] P.-J. Bristeau, P. Martin, E. Salaün, and N. Petit, "The role of propeller

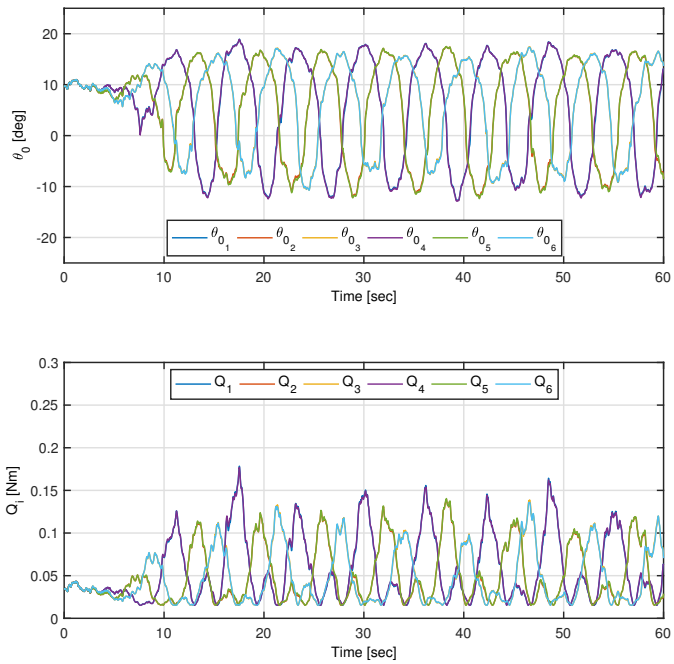

Fig. 15: Pitch and drag values by the VP-propellers, without using the optimization strategy (constant speed).

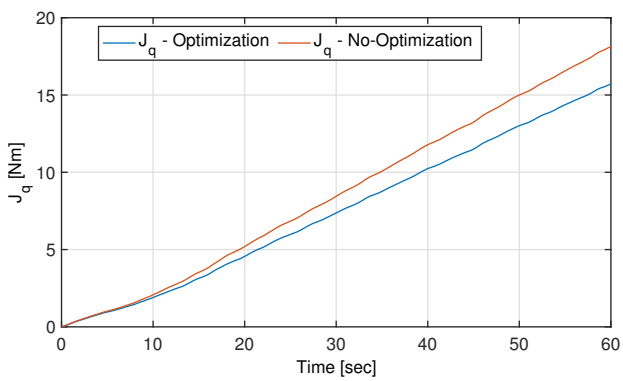

Fig. 16: Performance indexes of the two cases.

aerodynamics in the model of a quadrotor uav," in *Control Conference (ECC), 2009 European*. IEEE, 2009, pp. 683–688.

[10] E. Fresk and G. Nikolakopoulos, "Experimental model derivation and control of a variable pitch propeller equipped quadrotor," in *2014 IEEE Conference on Control Applications (CCA)*. IEEE, 2014, pp. 723–729.

[11] R. Cohen, D. Miculescu, K. Reilley, M. Pakmehr, and E. Feron, "Online performance optimization of a dc motor driving a variable pitch propeller," *arXiv preprint arXiv:1310.0133*, 2013.

[12] S. Sheng and C. Sun, "Control and optimization of a variable-pitch quadrotor with minimum power consumption," *Energies*, vol. 9, no. 4, p. 232, 2016.

[13] G. J. Leishman, *Principles of helicopter aerodynamics with CD extra*. Cambridge university press, 2006.

[14] R. W. Prouty, *Helicopter performance, stability, and control*. Krieger Publishing Company, 1995.

[15] A. Simha, S. Vadgama, and S. Raha, "Almost-global exponential tracking of a variable pitch quadrotor on se (3)," *IFAC-PapersOnLine*, vol. 50, no. 1, pp. 10 268–10 273, 2017.

[16] M. Faessler, D. Falanga, and D. Scaramuzza, "Thrust mixing, saturation, and body-rate control for accurate aggressive quadrotor flight," *IEEE Robotics and Automation Letters*, vol. 2, no. 2, pp. 476–482, 2017.

[17] A. Franchi and A. Mallet, "Adaptive closed-loop speed control of bldc motors with applications to multi-rotor aerial vehicles," in *IEEE International Conference on Robotics and Automation (ICRA)*, 2017.

[18] D. Simon, *Evolutionary optimization algorithms*. John Wiley & Sons, 2013.

[19] Electro-Craft Corp. USA, "Chapter 2 - DC Motors and Generators," in *DC Motors, Speed controls, Servo Systems: An Engineering Handbook.*, 3rd ed. Pergamon Press, 1977, pp. 2–1 – 2–114.

[20] S. Rajappa, M. Ryll, H. H. Bülthoff, and A. Franchi, "Modeling, control and design optimization for a fully-actuated hexarotor aerial vehicle with tilted propellers," in *IEEE International Conference on Robotics and Automation (ICRA)*, 2015.

Model id	Lift force (thrust) prediction and residual at 40, 50, 60, 70, and 80 Hz
i)	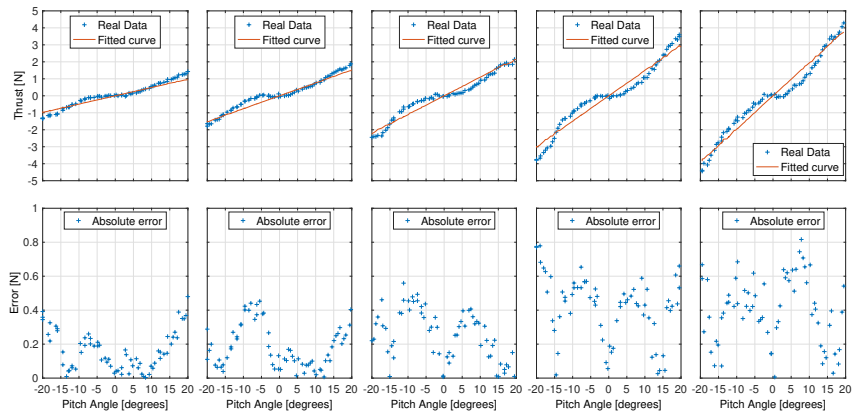
ii)	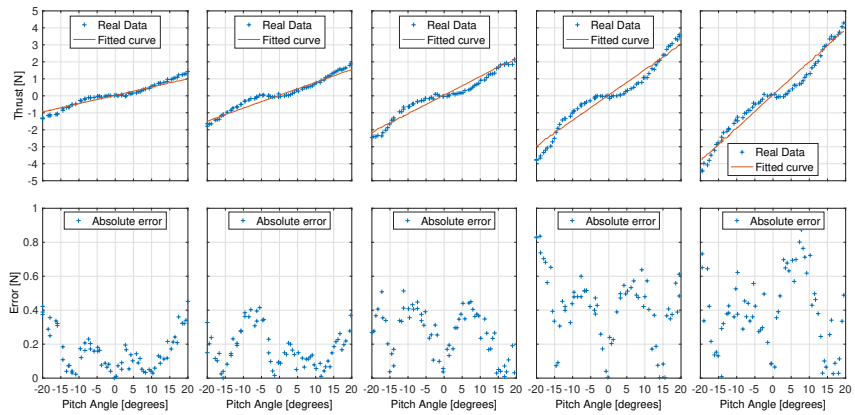
iii)	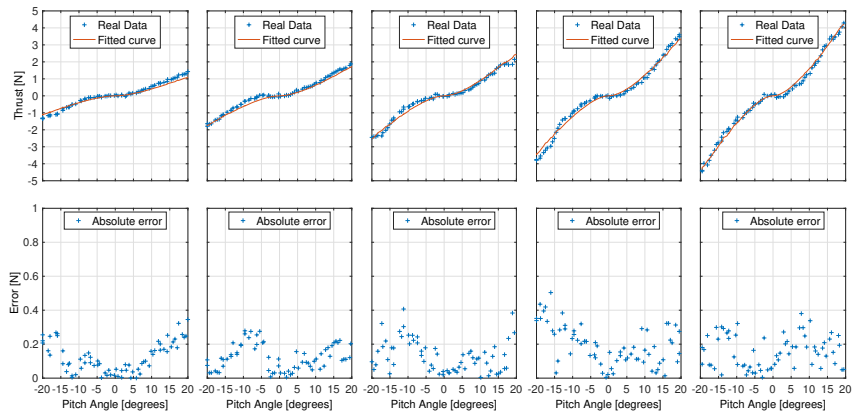
v) (proposed)	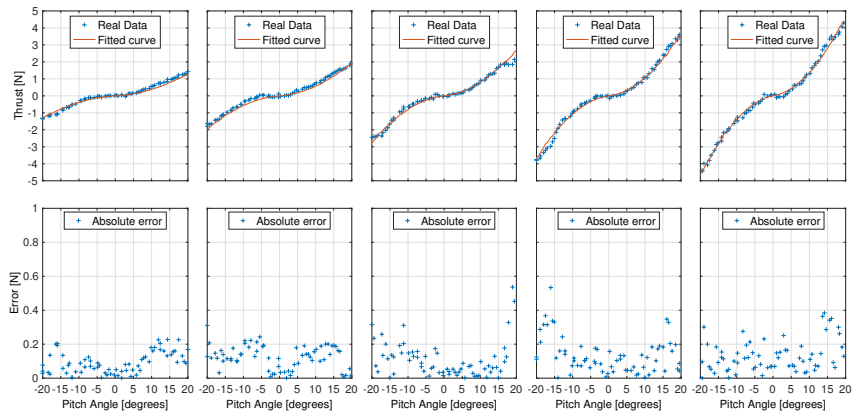

Fig. 17: Prediction vs measurements of the lift force (thrust) for models i), ii), iii), and the proposed model. The predicted lift of model iv) is very similar to the one of model iii) (see RMSE in Table III) and is not reported here for space considerations.

Model id	Drag moment prediction and residual at 40, 50, 60, 70, and 80 Hz
i)	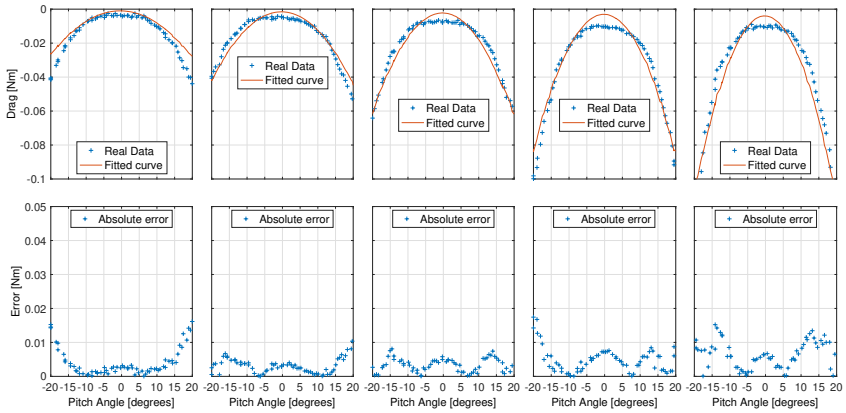
ii)	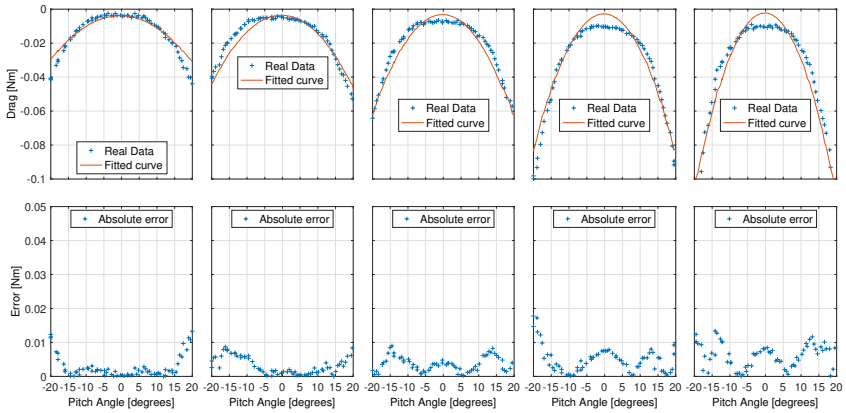
iii)	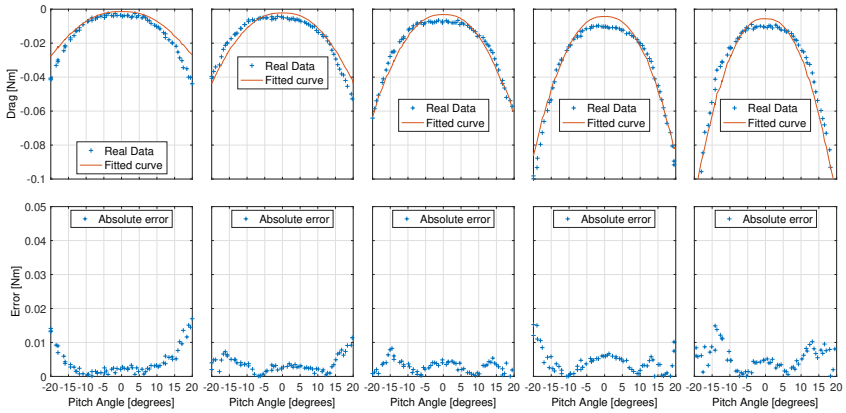
v) (proposed)	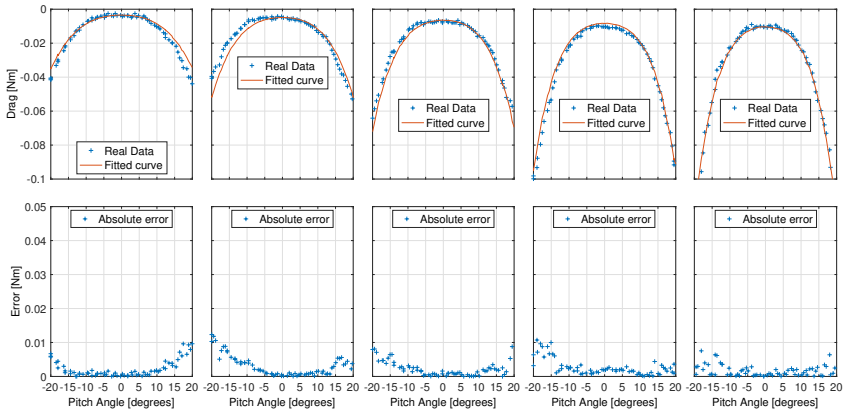

Fig. 18: Prediction vs measurements of the drag moment for models i), ii), iii), and the proposed model. Model iv) has no drag moment.